

Solution-Processed, Photo-Patternable Fluorinated Sol–Gel Hybrid Materials as a Bio-Fluidic Barrier for Flexible Electronic Systems

Injun Lee, Yong Ho Kim, Jinhyeong Jang, Kwang-Heum Lee, Junho Jang, Young-Woo Lim, Sang-Hee Ko Park, Chan Beum Park, Wonryung Lee,* and Byeong-Soo Bae*

Reports have recently been published on ultrathin biofluid barriers, which enable the long-term measurement of biological signals and exhibit conformability on nonlinear surfaces such as skin and organs. However, inorganic- and organic-based barriers have process incompatibility and high water permeability, respectively. Siloxane- (inorganic) based fluorinated epoxy (organic) hybrid materials (FEH) are demonstrated for bio-fluidic barrier and the biocompatibility and barrier performance for flexible electronic systems as solution-processed oxide thin-film transistors (TFTs) on 1.2 μm thick polyimide (PI) thin film substrate is confirmed. FEH thin film can be patterned as small as 10 μm through conventional photolithography. The fabricated solution-processed indium oxide TFTs with FEH barriers exhibit durable performance over 16 h with no dramatic change of transfer characteristics in phosphate-buffered saline (PBS) environment. Furthermore, to realize FEH barriers for flexible systems, the solution-processed indium oxide TFTs with FEH barriers on ultrathin PI substrate are demonstrated subjected to compression test and successfully measure the electrical properties with no irreversible degradation during 1000 cycles of mechanical testing in PBS.

1. Introduction

Barriers are key components of bio-integrated electronic devices, providing protection from the bio-fluidic environment and enabling high performance without degradation over time. The development of flexible and long-term stable bio-fluidic barriers allows the placement of flexible electronics on the skin

or organs, where they can sense biological indicators such as temperature,^[1,2] blood pressure,^[3,4] electrocardiogram (ECG),^[5,6] and glucose^[7,8] in real time; as such, barriers have become increasingly important, owing to their high potential for application in the area of health monitoring.^[9] Moreover, there has been progress in the design of flexible bio-integrated devices. The total thickness of ultra-thin bio-integrated devices has been reduced to less than 10 μm ;^[10–13] such ultra-thin devices enable improvement of conformability with the nonlinear curvature of biological tissues and noninvasive integration on soft tissues. Therefore, development of thin barriers of under a-few-micrometer scale has become important to carry out long-term operation of ultra-flexible electronics and to protect the underlying device against bio-fluids.


Bio-fluidic barriers based on inorganic and organic materials on ultrathin substrates have been widely investigated

for flexible bio-integrated devices. In general, the properties of barriers consisting of inorganic materials show pronounced superiority in water vapor and gas transmission rate values compared to those of organic-based barriers.^[14,15] In recent years, thin, flexible, and long-lived inorganic barriers to bio-fluid have been proposed using physically transferred layers of silicon oxide (t-SiO_2)^[16] and metal silicide (TiSi_2).^[17] Ultrathin, transferred layers of thermally grown t-SiO_2 are flexible, defect-free, and show low water permeability, resulting in device lifetimes of decades due to slow hydrolysis of t-SiO_2 (0.04–1.26 nm·per day in phosphate-buffered saline (PBS) at a pH 7.4, 37 °C). One study demonstrated that t-SiO_2 with highly doped silicon can be utilized as a conductive interface, simultaneously enabling excellent stability and conductive coupling to bio-tissues. To improve the limit lifetime of highly boron-doped silicon at conductive interfaces between flexible systems and bio-tissues, physically transferred TiSi_2 exhibits a lifetime three orders of magnitude higher than that of t-SiO_2 , and also acts as a bio-fluidic barrier for chronic implant systems.

Despite the high fluid permeability of organic layers, intensive investigation of flexible and reliable organic based bio-fluid barriers has been carried out, including polyimide (PI)^[18,19] and

I. Lee, Dr. Y. H. Kim, K.-H. Lee, Dr. J. Jang, Dr. Y.-W. Lim, Prof. S.-H. K. Park, Dr. W. Lee, Prof. B.-S. Bae
Wearable Platform Materials Technology Center
Korea Advanced Institute of Science and Technology
291 Daehak-ro, Yuseong-gu, Daejeon 34141, Republic of Korea
E-mail: wrlee@kaist.ac.kr; bsbae@kaist.ac.kr

I. Lee, Dr. Y. H. Kim, J. Jang, K.-H. Lee, Dr. J. Jang, Dr. Y.-W. Lim, Prof. S.-H. K. Park, Prof. C. B. Park, Dr. W. Lee, Prof. B.-S. Bae
Department of Materials Science and Engineering
Korea Advanced Institute of Science and Technology
291 Daehak-ro, Yuseong-gu, Daejeon 34141, Republic of Korea

 The ORCID identification number(s) for the author(s) of this article can be found under <https://doi.org/10.1002/aelm.201901065>.

DOI: 10.1002/aelm.201901065

SU-8^[20,21] due to their process compatibility. The high thermal stability and flexibility of PI is promising for use in bio-fluidic barrier materials for bio-integrated electronic applications.^[22,23] For example, a 1 μm thick PI barrier can be spin coated on the top of carbon nanotube inverters, amplifying the signal of ECG on the skin, resulting in high reliability against compression bending tests. Also, PI barriers do not exhibit deterioration due to bio-fluids or mechanical stress during ablation or detection measurements in balloon catheters, therefore it can be used for cardiac electrophysiological mapping and ablation therapy.^[18] Barrier materials that simultaneously exhibit photopatternability are attractive and can be applied to the fabrication of various structural layers of multi-layer devices, using simple fabrication methods and without additional etching process. SU-8 is a widely exploited epoxy-based negative photoresist designed for a large array of microelectronic systems; it has been utilized for bio-fluidic barriers recently due to its hydrophobicity, and chemical and thermal resistance.^[23] SU-8 barriers on graphene-based electrochemical devices for diabetes monitoring can measure sweat-based glucose and pH levels in real-time. Additionally, if they are used to perform a time-dependent stability test, the glucose sensor is reliable for 6 h when using artificial sweat.^[20]

However, these inorganic and organic materials for bio-fluidic barriers have certain problems, including process incompatibility and high water permeability, respectively. The thermal oxidation temperatures of t-SiO₂ and TiSi₂ are 1150 and 850 °C, which means that they cannot be grown on low temperature stable materials. Also, etching of inorganic materials is very hard because it requires a dry etching process or strong acid such as hydrofluoric acid.^[24] On the other hand, PI and SU-8 can be fabricated by simple low temperature processing, but high water permeability due to free volume of these organic materials makes them difficult to serve as bio-fluidic barrier enabling long-term stability of device.^[25] In order to improve these vulnerabilities of intrinsic material-based barriers, organic/inorganic multilayer encapsulation has been used to protect flexible organic light emitting diode (OLED) devices from oxygen and moisture^[26]; however, this method cannot deal with conformable conditions of biological tissue, which is located in bio-fluid for a long time.

In this work, we have successfully fabricated sol-gel derived fluorinated epoxy siloxane hybrimer (FEH) film, which exhibits a hydrophobic, photo-patternable, and durable bio-fluidic barrier. The fluorine functional group (organic), with random network structure induced by siloxane bonds (inorganic), provides highly condensed materials with water resistivity. Using ultra violet (UV) polymerization, FEH can be formed into well-defined micro-patterns via epoxide cationic ring opening mechanism. Compared to conventionally executed organic-based bio-fluid barriers, spin coated 1 μm thick films of FEH exhibit very low water penetration properties, as verified by measuring the remaining magnesium (Mg) under the barrier after soaking in the water. The results of electrical impedance spectroscopy measurements reveal a defect-free 1 μm thick FEH film, which is validated as stable and as having a low impedance interface in PBS environment. Furthermore, we demonstrate aqueous solution-processed indium oxide thin film transistors (TFTs) with an FEH barrier that exhibits transfer characteristics in the

PBS environment for 16 h without significant degradation. The good mechanical durability of the combination of oxide TFTs on ultrathin substrate indicates that solution-processable FEH is a promising barrier material for use in flexible and conformable bio-integrated devices.

2. Results and Discussion

Previously, sol-gel derived epoxy siloxane hybrimer (EH) films were reported for use in encapsulation of flexible OLED.^[27,28] Despite the high water vapor permeability of EH (1.09 gm^{-2} per day), the multi-barriers, which were composed of EH and MgO, were adequate for encapsulation of OLEDs, protecting them from oxygen and water vapor.

To enhance the water-resistance of high water vapor permeable EH films, fluorinated epoxy hybrimer (FEH) films are designed to take advantage of the inherent hydrophobicity of fluorinated compounds.^[29] Figure 1a presents a schematic illustration of the synthesis procedure of fluorinated epoxy oligo-siloxane (FEO) resin and FEH. Through non-hydrolytic sol-gel condensation, which is used to form a fully siloxane bonding (–Si–O–Si–) network between the three monomers, transparent FEO resin with a fluorine group is fabricated. The molecular structure of FEO is investigated by ²⁹Si-NMR to confirm the formation of the siloxane network, which is evidenced by the existence of the highly condensed Si species shown in Figure S1, Supporting Information. The FEO resin diluted with propylene glycol methyl ether acetate (PGMEA) is spin coated to fabricate 1 μm thick FEH thin film (Figure 1b). Cationic ring opening of FEO's epoxide is induced by UV irradiation for polymerization. To validate the presence of siloxane bonds, fluorine functional groups, and cross-linked FEH by epoxy ring opening polymerization, we analyzed the FEO resin and FEH films using Fourier transform infrared (FT-IR) spectroscopy (Figure 1c). Broad bands at 1000–1150 cm^{-1} are observed in both FEO resin and FEH films, indicating the existence of stretching of the siloxane bond after sol-gel reaction between the hydroxyl groups of diphenylsilanediol (PS) and the methoxide groups of 2-(3,4-epoxycyclohexyl) ethyltrimethoxysilane (ES) and trimethoxy(1H,1H,2H,2H-nonafluorohexyl) silane (FS). Moreover, bands corresponding to the C–F bond at 1200–1250 cm^{-1} of FS and epoxide bands at 870–890 cm^{-1} are observed for the FEO resin and FEH films. However, epoxide bands decrease in FEH films compared to FEO resin, which is attributed to the cross-linking between epoxy groups in the FEO resin by cationic ring-opening polymerization after UV curing. On the other hand, the intensity of the phenyl group peak remains constant irrespective of the UV exposure. Using these results, the degree of FEH polymerization is confirmed by the calculation of epoxy conversion degree (ECD).^[30] Detailed calculation of ECD is included in the Experimental Section. The ECD value is 93.89%, which indicates successful polymerization of FEH by UV curing. Figure S6, Supporting Information, is FT-IR spectra of 1 μm thick FEH films under the different UV exposure dose. Comparing the low exposure dose (60 mJ cm^{-2}) with the high exposure dose (2 J cm^{-2}), the intensity is high, which indicates the FEH film was not fully polymerized after the low exposure dose.^[31] Thus, to fully

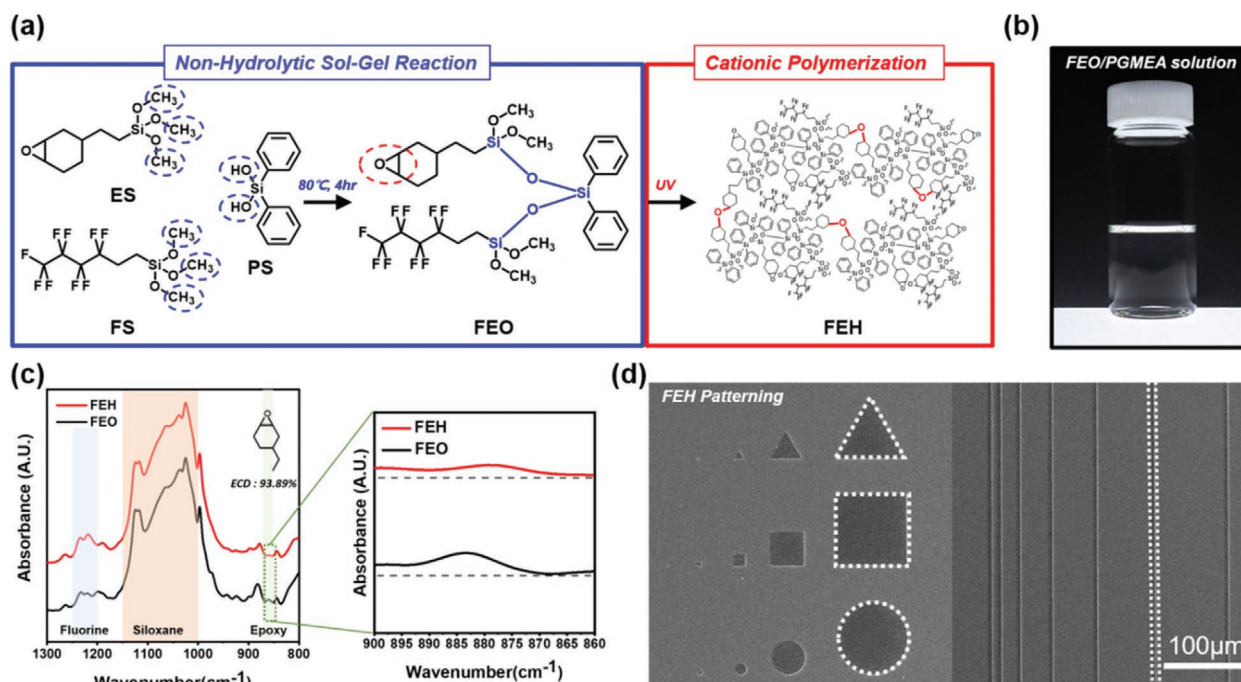


Figure 1. Synthesis and molecular structure of sol-gel processed FEO and photo-patternable FEH film. a) Synthesis procedure of fluorinated sol-gel hybrid materials. b) Digital photograph of FEO/PGMEA solution. c) FT-IR spectra of FEO resin and FEH film. d) SEM image of photo-patterned FEH.

polymerize FEH films, the high exposure dose (UV-A region, 2 J cm^{-2}) was induced.

UV-initiated cross-linking reactions are performed within $1 \mu\text{m}$ thick films; FEH can make a fine pattern, which is useful in multi-layer devices. The patterning process is described in the Experimental Section. The unexposed part can be removed by acetone and isopropanol, while the UV exposed part is insoluble in the developing solvent due to the polymerization of the epoxides. Various shapes, such as triangular, square, circle, and line, which have minimum sizes of $10 \mu\text{m}$, are used for demonstration. Figure 1d shows SEM images of well-defined patterns with $1 \mu\text{m}$ thickness. These results indicate that FEH thin film can be utilized as patternable passivation layer, which does not require additional dry etching process to make electrical connection between layers.

Mg test using Si wafer/ 100 nm thick Mg/ $1 \mu\text{m}$ thick barrier structure, as shown in Figure S2, Supporting Information, was utilized to confirm the water penetration of the films.^[16,32,33] The rapid reactivity of Mg with water [$\text{Mg} + 2\text{H}_2\text{O} \rightarrow \text{Mg}(\text{OH})_2 + \text{H}_2$] is induced by defects of the film; thus, it can be easily detected by optical microscopy. Conventionally used organic barriers, such as EH, parylene, PI, and SU-8, were also subjected to Mg testing. The area portion of defects, formed in the reaction of Mg, is calculated using an image analysis program (ImageJ) capable of measuring color change. Figure 2a shows sequential images of barrier films soaked in water at $25 \text{ }^\circ\text{C}$. Mg layers served as sensors to detect the penetration of water through the defects of the barrier films. Figure 2b shows a plot of amounts of remaining Mg under barrier films versus time plot of Mg soaking test. After 5 days, the FEH preserved 95% of Mg. Both the EH and parylene barriers revealed only 60% of remaining Mg after 5 days. Mg samples encapsulated by SU-8 and PI

barrier films were observed to decrease quickly within only 1 and 3 days, respectively. Furthermore, to investigate the hydrophobicity of FEH and other organic-based barrier films, measurement of water contact angle was performed (Figure 2c). The FEH film shows excellent hydrophobicity, with a water contact angle of 100° . The EH, a fluorine-free siloxane epoxy hybrimer, showed a water contact angle of 80° . The water contact angle of the Parylene, PI, and SU-8 films were low at 96° , 71° , and 63° , respectively (Figure S3, Supporting Information). From these results, the water resistivity of highly hydrophobic FEH is superior to those of other conventional organic-based barrier materials. Also, the Mg soaking test in the PBS at $37 \text{ }^\circ\text{C}$ was performed for 5 days, as shown in Figure S4, Supporting Information. After 5 days, the preserved Mg under FEH, EH barrier in the PBS are 98.53%, 86%, respectively. It shows the outstanding barrier properties of FEH barrier in the biofluid environment.

The biocompatibility of the FEH films was confirmed by culturing the rat cardiomyocyte (H9c2) as shown in Figure 3a. We assessed the proliferation activities of H9c2 on the FEH films using the Cell Counting Kit-8 (CCK-8).^[34,35] After culturing for 3 and 7 days, the number of living cells on the FEH films increased significantly, which indicated that the sol-gel processed FEH was favorable for cell proliferation (Figure 3b). We further verified the non-cytotoxicity of the FEH films using the LIVE/DEAD assay method (Figure 3c).^[36] According to the results of LIVE/DEAD assay, H9c2 cells attached to FEH films and exhibited complete viability at 3 and 7 days of cultivation. Thus, the CCK-8 result confirms that the sol-gel processed FEH is biocompatible material, enabling application of biofluidic barrier.

To demonstrate the barrier properties of FEH in a biofluidic environment, solution-processed aqueous indium oxide

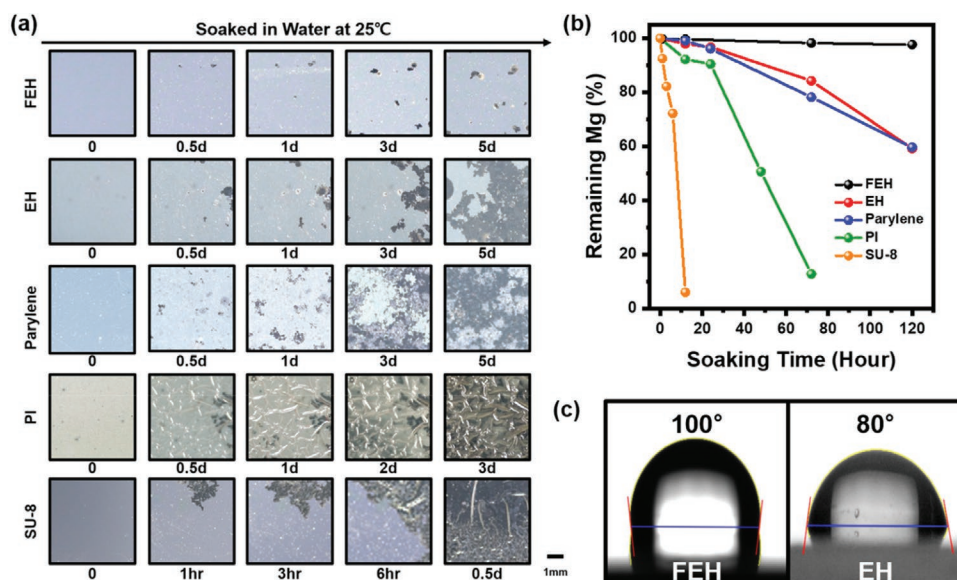


Figure 2. Water barrier evaluation of FEH, compared to other organic films, using Mg soaking test and water contact angle measurement. a) Sequential images of Mg passivated by 1 μm thick layers of FEH, EH, parylene, PI, and SU-8 soaked in DI water at 25 $^{\circ}\text{C}$. b) Graph showing area of residual Mg versus time plot. c) Water contact angles of FEH and EH.

TFTs^[37] are fabricated and tested in a bio-fluidic environment (Figure 4a). Adsorption of water on metal oxide serves to form donor-like traps, resulting in a negative shift of threshold voltage.^[38] Thus, even when there is micro-scale defect of the barrier film, the performance of the oxide TFTs is easily affected

by water penetration.^[39] Figure 4b is a schematic of the device structure of the solution-processed indium oxide TFT with FEH barrier under PBS droplet. Figure 4c shows the transfer curve of solution-processed indium oxide TFTs in the PBS environment. Before soaking in PBS, the mobility (μ) of TFTs was

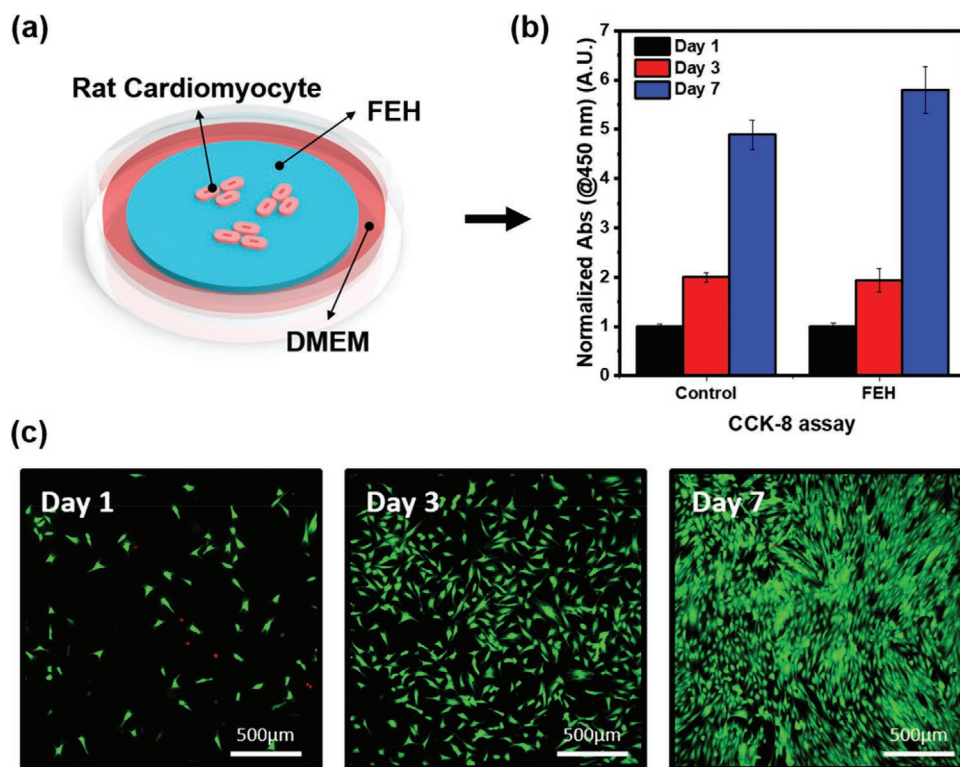


Figure 3. In vitro biocompatibility of FEH film. a) The schematic of in vitro biocompatibility test of FEH using rat cardiomyocytes (H9c2). b) CCK-8 assay result of H9c2 cells on FEH compared with control films after 1, 3, and 7 days. Data are presented as the mean \pm standard deviation ($n = 4$). c) The fluorescent images of live (green) and dead (red) cells cultured on FEH film. The cells were imaged after 1, 3, and 7 days of culture.

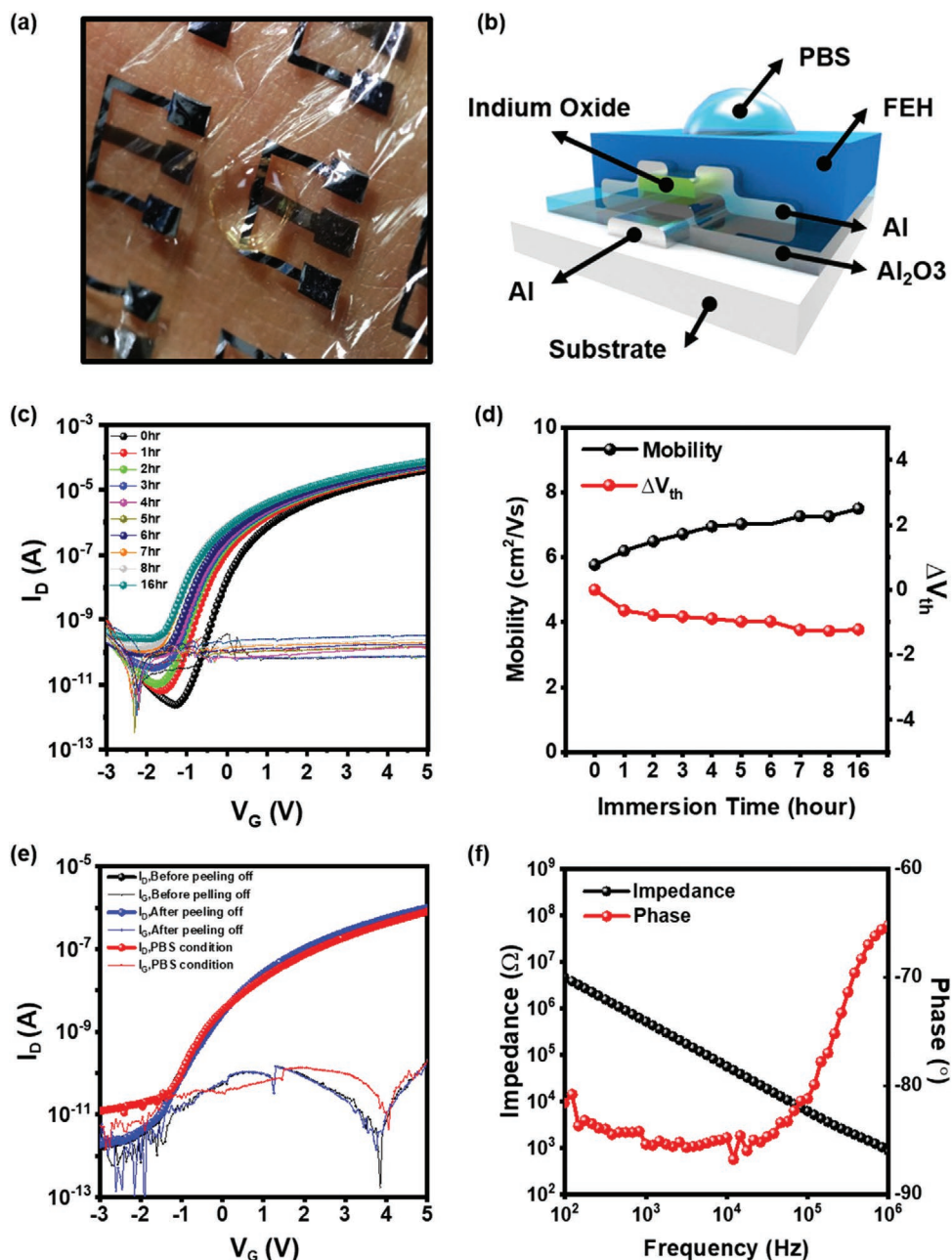


Figure 4. Electrical characteristics of 1 μm thick FEH film in PBS environment. a) Digital photograph of ultra-thin device under PBS droplet. b) Schematic illustration of cross-sectional structure of solution-processed indium oxide TFTs with FEH barrier under PBS droplet. c) Transfer curves measured with PBS drop on device at applied drain voltage of 5 V. Tests with PBS solutions indicate that failure occurs after 16 h. d) Plot of mobility and change of threshold voltage of indium oxide TFTs in PBS condition as function of soaking time. e) Transfer curves measured for ultra-thin device before and after peeling off from rigid substrate and under PBS droplet at applied drain voltage of 5 V. f) Electrochemical impedance spectra of FEH layer.

5.77 $\text{cm}^2 \text{V}^{-1} \text{s}^{-1}$, threshold voltage (V_{th}) was 0.01 V, and on/off current value was $\approx 10^6$. As can be seen in Figure 4d, TFTs showed good electrical stability in the PBS environment for 16 h. Increase of mobility (1.7 $\text{cm}^2 \text{V}^{-1} \text{s}^{-1}$) and negative shift of threshold voltage (-1.2 V) were observed. Therefore, the FEH films show durable bio-fluidic barrier performance, confirmed by the stable electrical characteristics of the oxide TFTs for 16 h.

To further verify the barrier performance of FEH bio-fluidic barrier for flexible electronic systems, we fabricated

solution-processed indium oxide TFTs on 1 μm thick PI films with a FEH barrier. A poly(methyl methacrylate) (Sigma-Aldrich, PMMA) layer was deposited as a sacrificial layer, which facilitated delamination of the ultra-thin device on the 1 μm thick PI substrates from carrier substrate (Figure S5, Supporting Information). Figure 4e shows the transfer curve of solution-processed indium oxide TFTs on 1.2 μm thick PI substrates before and after peeling off process. There is no significant degradation in TFT performance before or after peeling

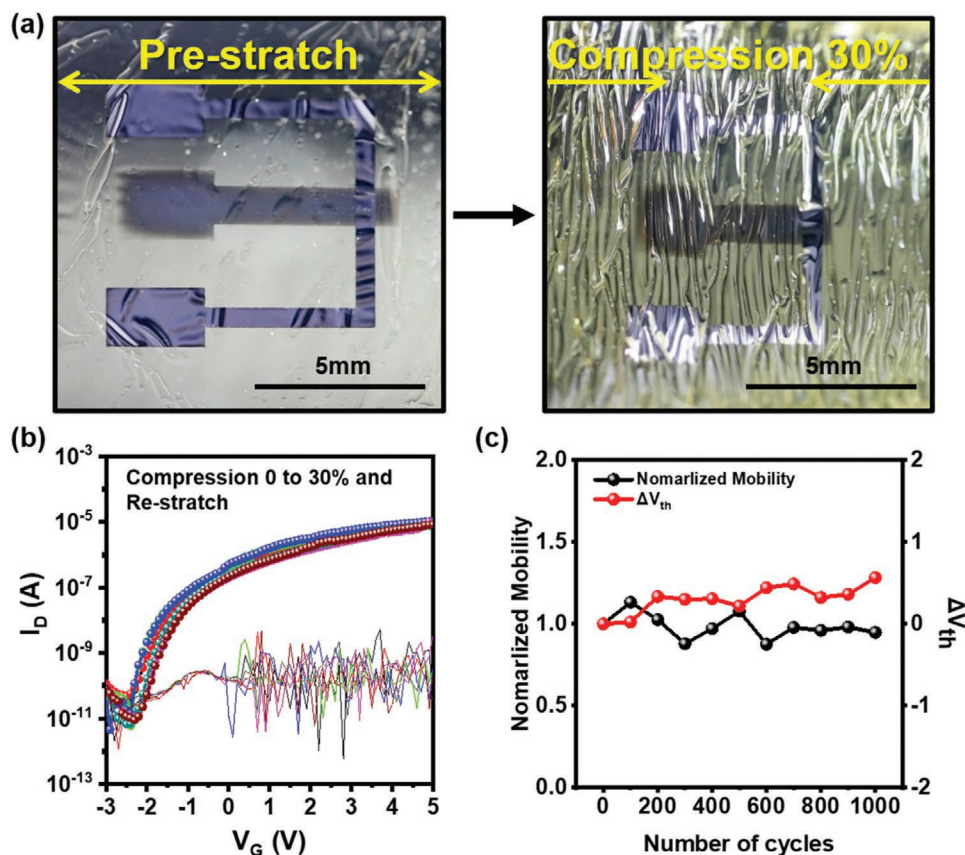


Figure 5. Mechanical durability test of ultra-thin device with FEH barrier in the PBS. a) Digital photograph of ultra-thin TFT device with FEH barrier when elastomer is pre-stretched and compressed to 30%. b) Transfer characteristics of ultra-thin TFT device under PBS droplet after compression and re-stretched at applied drain voltage of 5 V. c) Plot of normalized mobility (black) and change of threshold voltage (red) during 1000 cycles of repeated 30% compression and re-stretch to original state under PBS droplet.

off from the rigid substrate. In the case of under-PBS operation (Figure 4e), the stable electrical properties, such as mobility ($0.06 \text{ cm}^2 \text{ V}^{-1} \text{ s}^{-1}$) and on/off value ($\approx 10^4$), of the indium oxide TFT with FEH barrier are also verified. These results indicate that indium oxide TFTs with FEH barrier on ultra-thin substrate have no significant change in electrical characteristics even when applying mechanical stress during the peeling off process and under PBS condition.

Furthermore, electrochemical impedance spectroscopy (EIS) was performed to check the barrier performance of FEH in the PBS environment. Figure 4f shows the magnitude of the impedance and the phase angle of electrodes (AC potential of 10 mV, frequency range of 1– 10^6 Hz, 0.1 M PBS solution). Slope of the plot of the impedance as function of frequency exhibits a value of -1 , which indicates high stability in response. In other words, FEH is well formed with no defects, and so the signal is not corrupted by resistive leakage. The phase rises to -65 at 10^6 Hz as the solution resistance begins to contribute to the response.

Mechanical durability of the solution-processed indium oxide TFTs with FEH barrier on ultra-thin substrate is required to ensure stable performance of electronic systems on human tissue or skin. Figure 5a is photograph of indium oxide TFTs with FEH barrier on PI substrate subjected to compression test. The fabricated indium oxide TFTs with FEH barrier on

the carrier substrate were peeled off and laminated onto a pre-stretched elastomer film (KTD-19, 3M). As the pre-stretched elastomer film is relaxed to original state, the devices on ultra-thin substrate form random networks of wrinkles to accommodate the compression strain. As shown in Figure 5b, the indium oxide TFTs show stable electrical characteristics at an almost identical level during compression and release with 10% compressive strain steps under PBS droplet. Subsequently, we measured the transfer characteristics when devices were subjected to repeated 30% compression and release to the original state under PBS droplet. Figure 5c shows normalized mobility and change of threshold voltage during repeated compression to 30% and re-stretching to original state under PBS droplet. With repetitive compression cycling, the maximum change of mobility percentage and threshold voltage were 13% and 0.56 V, respectively. No irreversible degradation of electrical properties was observed during 1000 cycles of mechanical testing under PBS droplet.

3. Conclusion

In this work, we demonstrate a sol-gel derived fluorinated epoxy hybri-mer for use as a bio-fluidic barrier in solution processes. Photo-patternable FEH can be micro-patterned, with

features as small as 10 μm . Due to the fluorine functional group, FEH has superior water resistivity and hydrophobicity compared to other organic films, which is verified by magnesium soaking test and water contact angle measurement. Also, we confirmed that FEH is a biocompatible material through in vitro biocompatibility test using rat cardiomyocytes. To demonstrate FEH as a bio-fluidic barrier, we fabricated solution oxide TFTs with FEH barrier layer and measured the transfer characteristics of oxide TFTs in the PBS environment. The oxide TFTs with FEH barrier exhibit durable performance during 16 h, with no dramatic change of electrical properties in PBS environment. To evaluate the electrical stability of the barrier in a bio-fluidic environment, we use EIS analysis to confirm that FEH films exhibit no resistive leakage through defects and that they have high signal stability. Furthermore, indium oxide TFTs with FEH barriers on ultra-thin PI substrates demonstrate no degradation of electrical properties, even during 1000 repeated cycles of 30% compression and re-stretch under PBS droplet. We envision that our sol-gel processed FEH films will be utilized as bio-fluidic barriers for flexible and conformable electronics.

4. Experimental Section

Synthesis of Fluorinated Epoxy Oligo-Siloxane Resin: Fluorinated epoxy oligo-siloxane (FEO) resin was synthesized by non-hydrolytic sol-gel condensation of trimethoxy(1H,1H,2H,2H-nonafluorohexyl)silane (FS, Tokyo Chemical Industry), 2-(3,4-epoxycyclohexyl)ethyltrimethoxysilane (ES, Gelest) and diphenylsilanediol (PS, Gelest). Barium hydroxidemonohydrate ($\text{Ba}(\text{OH})_2 \cdot \text{H}_2\text{O}$, Sigma-Aldrich) was used as base catalyst. The content of experimented ES, FS, and DS was 35, 5, and 60 mol% of entire precursor, and the amount of $\text{Ba}(\text{OH})_2 \cdot \text{H}_2\text{O}$ was 0.2 mol% of entire precursor. The molar ratio of ES and FS to DS was decided to be 2:3 in order to synthesize highly condensed FEO resin.^[40] FS, ES, DS, and $\text{Ba}(\text{OH})_2 \cdot \text{H}_2\text{O}$ were reacted in a two-neck flask with a magnetic stirrer under 80 $^\circ\text{C}$ with N_2 gas purging for 4 h.

Spin Coating of Fluorinated Epoxy Hybrimer Film: Fabrication of 1 μm thick fluorinated epoxy hybrimer (FEH) film began with preparation of FEO resin diluted in propylene glycol methyl ether acetate (PGMEA, Sigma-Aldrich), of which the total weight ratio of FEO resin to PGMEA was 2:5. Triarylsulfonium hexafluoroantimonate salts (Sigma-Aldrich) were added to the FEO resin with PGMEA for initiating cationic ring-opening polymerization. The prepared solution was spin-coated at 3000 rpm for 30 s on substrate. To vaporize PGMEA, coated sample was annealed at 120 $^\circ\text{C}$ for 10 min in ambient condition. FEH film was obtained after UV curing (UV-A region, 2 Jcm^{-2}) for 5 min in ambient atmosphere. To further boost the polymerization of FEH film, UV-cured FEH film was annealed at 120 $^\circ\text{C}$ for 5 min.

Calculation of Epoxy Conversion Degree: From the FT-IR data before and after the UV curing process, ECD can be expressed in terms of the decrease of the epoxy group peak (870–890 cm^{-1}) relative to the unchanged phenyl group peak (1580–1590 cm^{-1}). ECD was calculated using the following equation.

$$\text{ECD (\%)} = 1 - \frac{\left(\frac{A_{\text{epoxy}}}{A_{\text{phenyl}}} \right)_{\text{After UV curing}}}{\left(\frac{A_{\text{epoxy}}}{A_{\text{phenyl}}} \right)_{\text{Before UV curing}}} \quad (1)$$

where A_{epoxy} and A_{phenyl} are area under the peak of the epoxy peak and area under the peak of the phenyl peak, respectively. FT-IR data were obtained using a JASCO FT/IR 4200.

UV Patterning of Fluorinated Epoxy Hybrimer: FEO coating resin was prepared by mixing FEO resin, PGMEA, and triarylsulfonium hexafluoroantimonate salts at a weight ratio of 50:125:1. The prepared solution was spin-coated and annealed at 120 $^\circ\text{C}$ for 10 min. Then, sample was exposed to UV through a photomask. After UV exposure, the sample was post-baked on a hotplate at 120 $^\circ\text{C}$ for 5 min. The sample was then developed with acetone and isopropanol to remove the uncured region.

In Vitro Biocompatibility Test of Fluorinated Epoxy Hybrimer: The H9c2 rat cardiomyocyte (ATCC, Manassas, VA, USA) was utilized to confirm the biocompatibility of the FEH films. Dulbecco's modified Eagle's medium (DMEM) was purchased from ATCC (USA). Fetal bovine serum and penicillin streptomycin were obtained from Gibco (Carlsbad, CA, USA) and Welgene (Korea), respectively. The cells were grown in complete growth medium (DMEM with 10% fetal bovine serum and 1% penicillin streptomycin) at a humidified environment with 5% CO_2 gas condition at 37 $^\circ\text{C}$. The biocompatibility of the FEH films was confirmed by Cell Counting Kit CCK-8 assay (Dojindo Corp, Japan) and LIVE/DEAD assay (LIVE/DEAD Viability/Cytotoxicity Kit, Invitrogen, USA). H9c2 cells were spread on the FEH films at a density of 20000 cells per well in a 12-well plate for LIVE/DEAD assay, and at a density of 2000 cells per well in a 96-well plate for CCK-8 assay. The result of CCK-8 assay was measured by a microplate reader (Victor 3, PerkinElmer Inc., USA) after 1, 3, and 7 days of cultivation. The CCK-8 assay was progressed with the following steps; addition of 10 μL of CCK-8 reagent into 90 μL of cell media, incubation for 3 h at 37 $^\circ\text{C}$, and measurement of absorbance at 450 nm. All values in CCK-8 assay represented the mean \pm standard deviation ($n = 4$). LIVE/DEAD assay labeled live and dead cells in green and red color, respectively. The photographs of LIVE/DEAD assay were obtained through a fluorescence microscope (Eclipse 80i, Nikon, Japan) after 1, 3, and 7 days of cultivation. The control was sterilized in polystyrene cell culture plate.

Magnesium Soaking Test for Evaluation of Water Barrier Property Compared with Conventional Materials: To fabricate 100 nm of magnesium (Mg) thin film, an e-beam evaporator was utilized. The Mg formed a 0.25 cm^2 area on a clean Si wafer. Using spin coating, 1 μm of each organic material and parylene ($(\text{C}_8\text{H}_7\text{Cl})_n$, KISCO) were deposited on Mg for the Mg soaking test.

Fabrication of 1 μm thick epoxy hybrimer (EH)^[41] film began with preparation of EO resin diluted in propylene glycol methyl ether acetate (PGMEA, Sigma-Aldrich), of which the total weight ratio of FEO resin to PGMEA was 2:5. The ES and DS were 40 and 60 mol% of entire precursor, respectively. And the amount of $\text{Ba}(\text{OH})_2 \cdot \text{H}_2\text{O}$ was 0.2 mol% of entire precursor. Triarylsulfonium hexafluoroantimonate salts (Sigma-Aldrich) were added to the EO resin with PGMEA for initiating cationic ring-opening polymerization. The prepared solution was spin-coated at 3000 rpm for 30 s on substrate for 1 μm . To vaporize PGMEA, coated sample was annealed at 120 $^\circ\text{C}$ for 10 min in ambient condition. EH film was obtained after UV curing. To further boost the polymerization of EH film, UV-cured EH film was annealed at 120 $^\circ\text{C}$ for 5 min. The 1 μm thick SU-8 (SU-8 2000, MicroChem) film was fabricated by the following steps; spin-coating at 1000 rpm for 30 s, soft baking at 95 $^\circ\text{C}$, UV curing, and hard baking at 95 $^\circ\text{C}$. The 1 μm thick PI film was fabricated by the following steps; preparing the PI solution (poly (pyromellitic dianhydride-co-4,4'-oxydianiline), amic acid solution, Sigma-Aldrich), spin-coating at 6000 rpm at 30 s, and annealing at 300 $^\circ\text{C}$ for 1 h through thermal imidization process. The 1 μm thick parylene film was fabricated using vacuum deposition equipment through vaporization, pyrolysis, and deposition process.^[42]

SU-8 (MicroChem), polyimide using poly(pyromellitic dianhydride-co-4,4'-oxydianiline), amic acid solution, Sigma-Aldrich), and cycloaliphatic epoxy hybrimer (EH)^[41] film were deposited by spin coating. Parylene film was deposited by chemical vapor deposition method. Mg samples with different types of encapsulation layers on Si wafer were soaked in water at room temperature. To calculate the percentage of remaining Mg, we used an image analysis program (ImageJ). At first, photos were converted to 8-bit gray scale image by ImageJ. Undissolved Mg has a color brighter than the color of the Si wafer, so that the bright area can

be measured by setting a color threshold of which the brightness is over 160 scales.

Impedance Measurements: For measurements of impedance of FEH a CHI660E (CH Instruments) was used. The experiments used an AC potential of 10 mV with a frequency range of 100 Hz–1 MHz. Electrochemical impedance spectroscopy measurements were performed with a three electrode system consisting of an Au working electrode, an Ag/AgCl reference electrode, and an Au counter electrode. PBS (pH 7.4) solution served as electrolyte at room temperature. Figure S7, Supporting Information, provides a schematic of the EIS measurement of FEH.

Fabrication of Indium Oxide Thin Film Transistors with FEH Barrier on Glass Wafer: A solution-processed indium oxide^[37] thin film transistor (TFT) with a bottom gate top contact structure was fabricated on glass wafer. A 45 nm thick aluminum (Al) gate electrode was deposited using an e-beam evaporator through a shadow mask on glass substrate. The 45 nm thick aluminum oxide (Al₂O₃) gate dielectric layers were deposited at 150 °C by atomic layer deposition (ALD). Aqueous solution containing 0.002 mol of indium nitrate hydrate (In(NO₃)₃·xH₂O, Sigma-Aldrich) in 10 mL of deionized water was spin-coated onto the substrates at 3000 rpm for 30 s. After annealing at 250 °C for 1 h in ambient condition, indium oxide active layers were patterned by photolithography with a positive photoresist (AZ nLOF 2035, MicroChem). The 50 nm thick Al was deposited by thermal evaporator through a shadow mask for source and drain electrodes. Then, using the abovementioned method, indium oxide TFTs were encapsulated with 1 μm of FEH. Due to the UV patternable FEH, source and drain electrodes were easily connected with the probes. To make the path to the gate electrodes, reactive ion etching (RIE, Scien Tech Inc.) with CF₄, O₂, and Ar mixed gas was used to remove the dielectric layers.

Fabrication of Indium Oxide Thin Film Transistors with FEH Barrier on Ultrathin Substrates: A poly(methyl methacrylate) (PMMA) solution for sacrificial layer was spin coated on a silicon oxide (SiO₂) wafer, followed by spin coating of a 1 μm thick polyimide layer [(Poly(pyromellitic dianhydride-co-4,4'-oxydianiline), amic acid solution, Aldrich)]. The curing temperature of the PI layer was 300 °C for 1 h. The fabrication process of the solution-processed indium oxide TFTs and the FEH barrier is the same as the abovementioned process on the glass wafer (Figure S5, Supporting Information).

Electrical Performance Measurement: The electrical properties of the fabricated solution-processed metal oxide TFTs with PBS (pH 7.4) droplet were measured on a probe station with a Keithley 4200A-SCS parameter analyzer. Transfer characteristics were measured as gate bias was swept from –3 to 5 V at 500 mV intervals with V_{DS} of 5 V. The mobility levels of the fabricated oxide TFTs were calculated under the assumption that a channel is composed of thin film defined by source and drain electrodes with channel length of 100 μm and width 500 μm. The mobility is extracted from the transfer characteristics using the follow equation.

$$\mu = \frac{\left(\frac{d\sqrt{I_D}}{dV_G}\right)^2}{0.5C_i \frac{W}{L}} \quad (2)$$

where I_D, V_G, C_i, W, and L are drain current, gate voltage, capacitance of the gate dielectric per unit area, channel width, and channel length, respectively.

Mechanical Durability Test of Ultrathin Device with FEH Barrier: Elastomeric tape (KTD-19, 3M) was placed between two compression jigs. The free-standing device was laminated onto a pre-stretched elastomer substrate. The fabricated oxide TFTs on ultrathin-substrate with FEH were carefully delaminated from the carrier substrate. Uniaxial compression and re-stretch were performed on the stretching jig. Using a controllable screw, the length of the elastomer could be increased or decreased. Electrical contacts were linked with metal wire and non-conductive tape. The compression was defined as (L₀ –sL)/L₀. Data on

electrical characteristics from mechanical durability test were recorded using a Keithley 4200A-SCS.

Supporting Information

Supporting Information is available from the Wiley Online Library or from the author.

Acknowledgements

The authors thank Hyung Jin Park and Jongbeom Ko for discussions about TFT fabrication. This work was supported by the Wearable Platform Materials Technology Center (WMC) (NRF-2016R1A5A1009926) and Creative Research Initiative Center (Grant No.: NRF-2015 R1A3A2066191) funded by National Research Foundation of Korea (NRF) Grant of the Korean Government (MSIP). The authors also thank the Korea Basic Science Institute (KBSI) for help with the ²⁹Si NMR spectral measurements.

Conflict of Interest

The authors declare no conflict of interest.

Keywords

bio-fluidic barrier, inorganic–organic hybrid materials, oxide thin film transistors, sol–gel processing

Received: September 30, 2019

Revised: December 7, 2019

Published online:

- [1] D. H. Kim, N. Lu, R. Ma, Y. S. Kim, R. H. Kim, S. Wang, J. Wu, S. M. Won, H. Tao, A. Islam, K. J. Yu, T. Il Kim, R. Chowdhury, M. Ying, L. Xu, M. Li, H. J. Chung, H. Keum, M. McCormick, P. Liu, Y. W. Zhang, F. G. Omenetto, Y. Huang, T. Coleman, J. A. Rogers, *Science* **2011**, 333, 838.
- [2] Y. Zhang, R. C. Webb, H. Luo, Y. Xue, J. Kurniawan, N. H. Cho, S. Krishnan, Y. Li, Y. Huang, J. A. Rogers, *Adv. Healthcare Mater.* **2016**, 5, 119.
- [3] J. Park, M. Kim, Y. Lee, H. S. Lee, H. Ko, *Sci. Adv.* **2015**, 1, e1500661.
- [4] R. C. Webb, Y. Ma, S. Krishnan, Y. Li, S. Yoon, X. Guo, X. Feng, Y. Shi, M. Seidel, N. H. Cho, J. Kurniawan, J. Ahad, N. Sheth, J. Kim, J. G. TaylorVI, T. Darlington, K. Chang, W. Huang, J. Ayers, A. Gruebele, R. M. Pielak, M. J. Slepian, Y. Huang, A. M. Gorbach, J. A. Rogers, *Sci. Adv.* **2015**, 1, e1500701.
- [5] R. A. Nawrocki, H. Jin, S. Lee, T. Yokota, M. Sekino, T. Someya, *Adv. Funct. Mater.* **2018**, 28, 1803279.
- [6] K. I. Jang, H. U. Chung, S. Xu, C. H. Lee, H. Luan, J. Jeong, H. Cheng, G. T. Kim, S. Y. Han, J. W. Lee, J. Kim, M. Cho, F. Miao, Y. Yang, H. N. Jung, M. Flavin, H. Liu, G. W. Kong, K. J. Yu, S. Il Rhee, J. Chung, B. Kim, J. W. Kwak, M. H. Yun, J. Y. Kim, Y. M. Song, U. Paik, Y. Zhang, Y. Huang, J. A. Rogers, *Nat. Commun.* **2015**, 6, 6566.
- [7] A. J. Bandothkar, P. Gutruf, J. Choi, K. Lee, Y. Sekine, J. T. Reeder, W. J. Jeang, A. J. Aranyosi, S. P. Lee, J. B. Model, R. Ghaffari, C.-J. Su, J. P. Leshock, T. Ray, A. Verrillo, K. Thomas, V. Krishnamurthi,

- S. Han, J. Kim, S. Krishnan, T. Hang, J. A. Rogers, *Sci. Adv.* **2019**, *5*, eaav3294.
- [8] X. You, J. J. Pak, *Sens. Actuators, B* **2014**, *202*, 1357.
- [9] Y. Liu, M. Pharr, G. A. Salvatore, *ACS Nano* **2017**, *11*, 9614.
- [10] S. Park, S. W. Heo, W. Lee, D. Inoue, Z. Jiang, K. Yu, H. Jinno, D. Hashizume, M. Sekino, T. Yokota, K. Fukuda, K. Tajima, T. Someya, *Nature* **2018**, *561*, 516.
- [11] D. H. Kim, J. Viventi, J. J. Amsden, J. Xiao, L. Vigeland, Y. S. Kim, J. A. Blanco, B. Panilaitis, E. S. Frechette, D. Contreras, D. L. Kaplan, F. G. Omenetto, Y. Huang, K. C. Hwang, M. R. Zakin, B. Litt, J. A. Rogers, *Nat. Mater.* **2010**, *9*, 8.
- [12] M. Kaltenbrunner, T. Sekitani, J. Reeder, T. Yokota, K. Kuribara, T. Tokuhara, M. Drack, R. Schwödiauer, I. Graz, S. Bauer-Gogonea, S. Bauer, T. Someya, *Nature* **2013**, *499*, 458.
- [13] W. Lee, S. Kobayashi, M. Nagase, Y. Jimbo, I. Saito, Y. Inoue, T. Yambe, M. Sekino, G. G. Malliaras, T. Yokota, M. Tanaka, T. Someya, *Sci. Adv.* **2018**, *4*, eaau2426.
- [14] P. E. Burrows, G. L. Graff, M. E. Gross, P. M. Martin, M. K. Shi, M. Hall, E. Mast, C. Bonham, W. Bennett, M. B. Sullivan, *Displays* **2001**, *22*, 65.
- [15] M. D. Groner, S. M. George, R. S. McLean, P. F. Carcia, *Appl. Phys. Lett.* **2006**, *88*, 051907.
- [16] H. Fang, J. Zhao, K. J. Yu, E. Song, A. B. Farimani, C.-H. Chiang, X. Jin, Y. Xue, D. Xu, W. Du, K. J. Seo, Y. Zhong, Z. Yang, S. M. Won, G. Fang, S. W. Choi, S. Chaudhuri, Y. Huang, M. A. Alam, J. Viventi, N. R. Aluru, J. A. Rogers, *Proc. Natl. Acad. Sci. USA* **2016**, *113*, 11682.
- [17] J. Li, R. Li, H. Du, Y. Zhong, Y. Chen, K. Nan, S. M. Won, J. Zhang, Y. Huang, J. A. Rogers, *ACS Nano* **2019**, *13*, 660.
- [18] J. H. Koo, S. Jeong, H. J. Shim, D. Son, J. Kim, D. C. Kim, S. Choi, J. I. Hong, D. H. Kim, *ACS Nano* **2017**, *11*, 10032.
- [19] J. Viventi, D. H. Kim, L. Vigeland, E. S. Frechette, J. A. Blanco, Y. S. Kim, A. E. Avrin, V. R. Tiruvadi, S. W. Hwang, A. C. Vanleer, D. F. Wulsin, K. Davis, C. E. Gelber, L. Palmer, J. Van Der Spiegel, J. Wu, J. Xiao, Y. Huang, D. Contreras, J. A. Rogers, B. Litt, *Nat. Neurosci.* **2011**, *14*, 1599.
- [20] H. R. Cho, D.-H. Kim, T. Hyeon, Y. S. Hong, S. H. Choi, C. Song, T. Kang, H. Lee, K. Shin, M. S. Kim, *Sci. Adv.* **2017**, *3*, e1601314.
- [21] J. Viventi, D. H. Kim, J. D. Moss, Y. S. Kim, J. A. Blanco, N. Annetta, A. Hicks, J. Xiao, Y. Huang, D. J. Callans, J. A. Rogers, B. Litt, *Sci. Transl. Med.* **2010**, *2*, 24ra22.
- [22] T. Stieglitz, H. Beutel, M. Schuettler, J.-U. Meyer, *Biomed. Microdevices* **2000**, *2*, 283.
- [23] C. Hassler, T. Boretius, T. Stieglitz, *J. Polym. Sci., Part B: Polym. Phys.* **2011**, *49*, 18.
- [24] J. Bühler, F. P. Steiner, H. Balthes, *J. Micromech. Microeng.* **1997**, *7*, R1.
- [25] K. Zhang, Q. Yu, L. Zhu, S. Liu, Z. Chi, X. Chen, Y. Zhang, J. Xu, *Polymers* **2017**, *10*, 1.
- [26] J. S. Lewis, M. S. Weaver, *IEEE J. Sel. Top. Quantum Electron.* **2004**, *10*, 45.
- [27] Y. C. Han, E. G. Jeong, H. Kim, S. Kwon, H. G. Im, B. S. Bae, K. C. Choi, *RSC Adv.* **2016**, *6*, 40835.
- [28] E. Kim, Y. Han, W. Kim, K. C. Choi, H. G. Im, B. S. Bae, *Org. Electron. Phys., Mater. Appl.* **2013**, *14*, 1737.
- [29] J. C. Biffinger, H. W. Kim, S. G. DiMagno, *ChemBioChem* **2004**, *5*, 622.
- [30] J. V. Crivello, R. Malik, *J. Polym. Sci., Part A: Polym. Chem.* **1997**, *35*, 407.
- [31] G. Choi, J. Jin, D. Shin, Y. H. Kim, J. Ko, *Adv. Mater.* **2017**, *29*, 1700205.
- [32] E. Song, R. Li, X. Jin, H. Du, Y. Huang, J. Zhang, Y. Xia, H. Fang, Y. K. Lee, K. J. Yu, J. K. Chang, Y. Mei, M. A. Alam, Y. Huang, J. A. Rogers, *ACS Nano* **2018**, *12*, 10317.
- [33] E. Song, Y. K. Lee, R. Li, J. Li, X. Jin, K. J. Yu, Z. Xie, H. Fang, Y. Zhong, H. Du, J. Zhang, G. Fang, Y. Kim, Y. Yoon, M. A. Alam, Y. Mei, Y. Huang, J. A. Rogers, *Adv. Funct. Mater.* **2018**, *28*, 1702284.
- [34] B. Maharjan, D. Kumar, G. P. Awasthi, D. P. Bhattarai, J. Y. Kim, C. H. Park, C. S. Kim, *Composites, Part B* **2019**, *177*, 107415.
- [35] M. Zhang, J. Zhu, X. Qin, M. Zhou, X. Zhang, Y. Gao, T. Zhang, D. Xiao, W. Cui, X. Cai, *ACS Appl. Mater. Interfaces* **2019**, *11*, 30631.
- [36] J. Jang, C. Cha, *Biomacromolecules* **2018**, *19*, 691.
- [37] Y. H. Hwang, J. Seo, J. M. Yun, H. Park, S. Yang, S. K. Park, B. Bae, *NPG Asia Mater.* **2013**, *5*, e45.
- [38] J. S. Park, J. K. Jeong, H. J. Chung, Y. G. Mo, H. D. Kim, *Appl. Phys. Lett.* **2008**, *92*, 2006.
- [39] S. Choi, J. Jo, J. Kim, S. Song, J. Kim, S. K. Park, Y. Kim, *ACS Appl. Mater. Interfaces* **2017**, *9*, 26161.
- [40] S. Yang, S. Y. Kwak, J. Jin, B. S. Bae, *ACS Appl. Mater. Interfaces* **2009**, *1*, 1585.
- [41] S. Yang, S. Y. Kwak, J. Jin, J. S. Kim, Y. Choi, K. W. Paik, B. S. Bae, *J. Mater. Chem.* **2012**, *22*, 8874.
- [42] T. Y. Chang, V. G. Yadav, S. De Leo, A. Mohedas, B. Rajalingam, C. L. Chen, S. Selvarasah, M. R. Dokmeci, A. Khademhosseini, *Langmuir* **2007**, *23*, 11718.